Towards guidelines for consistent wave propagation in CFD simulations

Stéphane RAPUC [a], Pierre CREPIER [a], Frédérick JAOUEN [a], Tim BUNNIK [a] and Pauline REGNIER [b]
[b] *Maritime Research Institute Netherlands, Wageningen, The Netherlands*
[b] *MARIN Academy / ENSTA Bretagne, Brest, France*

Abstract. Accurate prediction of structures and vessels motion at sea is critical to guarantee the safety and comfort of passengers on board, but also to understand the underlying physics of the derived quantities such as added resistance in waves. In this paper, a grid topology based on linear wave theory is proposed to efficiently and accurately propagate waves in a CFD domain. The grid topology consists of 3 refinement zones used to capture respectively the air-water interface, 90% and 99.9% of the wave kinetic energy. The performed sensitivity study showed that the error on wave dispersion, dissipation and reflection can all be contained within 2% using reasonable number of cells per wave length and amplitude. An application to the prediction of the motions of a 2D hull section in beam-on seas shows that using the guidelines derived lead to a good agreement with the results of a potential flow code, under the condition that the wave reflections are under control.

Keywords. CFD, URANS, wave generation, propagation, absorption, reflection, ReFRESCO

1. Introduction

Accurate prediction of motions of ships and structures at sea is critical to guarantee the safety and comfort of passengers on board, but also to understand the underlying physics of the derived quantities such as added resistance in waves or drift forces. While CFD simulations in calm water have been become standard practice the last years, simulations of vessels in waves are still challenging. Part of the difficulty lies in the fact that such simulations require an accurate propagation of the waves through the domain. The numerical settings should be such that the dissipation and dispersion of the waves as well as reflections on the domain boundaries are minimized.

In this paper, a computational efficient topology is proposed to generate unstructured grids for simulations in waves. This grid topology is derived from linear theory considerations. Using two-dimensional unsteady computations with the URANS solver ReFRESCO [1], the wave dispersion, dissipation and reflections obtained for the proposed numerical settings are extensively investigated. The numerical studies are carried out for both zero-speed and with forward speed, and both for deep water and shallow water.

Once the performance of the proposed numerical settings have been demonstrated for a wave propagating in an empty domain, the established guidelines are applied to calculate the motions of a 2D hull section in beam-on waves. In this study the effect of the methods used to absorb the waves at the boundaries and therefore minimize the effect of reflections on the calculated motions are demonstrated.

2. Theoretical background

2.1. Grid generation method

When a simulation involves the propagation of waves through the computational domain, a common practice is to define a region of increased cell density near the free-surface. In this region a certain number of cells per wave length and per wave height is then given, but no further details are provided ([4],[5]). Such a grid generation method heavily depends on how the grid generation software increases the cell size to provide space resolution further away from this narrow region. In this paper, it is proposed to establish guidelines based on the linear wave theory, which describes the wave orbital velocity field as follow:

$$\left.\begin{aligned} v_x &= z_a w \cdot e^{kz} \sin(wt + kx) \\ v_z &= z_a w \cdot e^{kz} \cos(wt + kx) \end{aligned}\right\} v = \sqrt{v_x^{\,2} + v_y^{\,2}} = z_a w \cdot e^{kz} \qquad (2.1.1)$$

With v the orbital velocity, v_x its projection in the wave direction, and v_z its vertical projection, z being the vertical position below the free surface, and ζ_a, ω and k representing respectively the wave amplitude, the wave frequency, and the wave number. Equation 2.1.1 shows that while the wave amplitude defines the magnitude of the orbital velocities, the orbital velocity decreases as function of the depth and the wave number. This indicates that space resolution is not only important near the free-surface, but also deeper below it, and that the appropriate depth up to which grid refinement is relevant depends on the wave length rather than the wave amplitude. The local cumulative kinetic energy as function as the water depth can be expressed as follows, where ρ is the water density per m:

$$E_k(z) = \frac{1}{2} r \int_z^0 v^2 = \frac{1}{4} r \frac{z_a^{\,2} w^2}{k} [1 - e^{2kz}] = \frac{1}{4} r g z_a^{\,2} [1 - e^{2kz}] \qquad (2.1.2)$$

Figure 1 gives a visual impression of the orbital velocity and cumulative kinetic energy as function of the water depth over one wave length derived from equations (2.1.1) and (2.1.2). In particular, one can see that to capture 90% and 99.9% of the kinetic energy, it is required to solve accurately the velocity field up to, respectively, 20% and 60% of the wave length below the undisturbed free-surface.

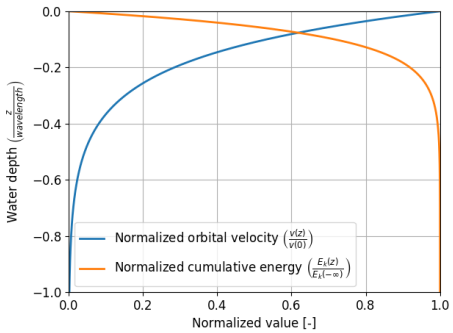

Figure 1 Normalized orbital velocity and cumulative energy as function of water depth

Based on these guidelines, a grid topology is derived, consisting of three main refinement zones (see also **Figure 2**):

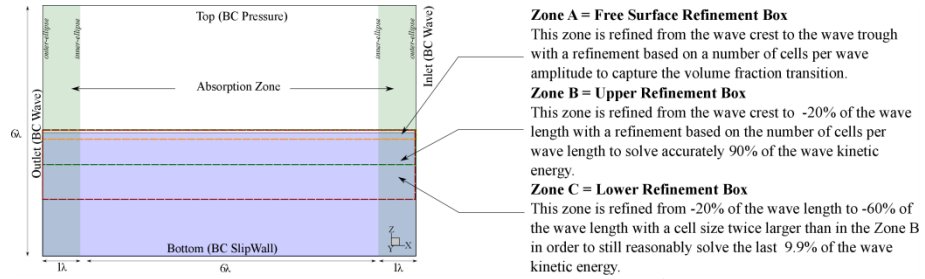

Figure 2 computational domain, boundary conditions and refinement zones

2.2. Wave generation / absorption

Dirichlet boundary conditions are imposed on the domain boundaries for the momentum and the air volume fraction equations. The water particle velocities and volume of fluid of the undisturbed incident wave are prescribed, including the effect of the forward speed when applicable.

Absorption zones are defined adjacent to the outer boundaries in order to avoid waves from reflecting from the domain boundaries and from propagating back in the domain. In the absorbing zones, body forces are applied in the momentum equations. These body forces are proportional to the difference between the expected undisturbed wave orbital velocities and the actual velocities from the CFD simulation:

$$\frac{\partial(\rho u_i)}{\partial t} + \frac{\partial(\rho u_j u_i)}{\partial x_j} = -\frac{\partial(p)}{\partial x_i} + \frac{\partial(\tau_{ij})}{\partial x_j} + \rho g_i + \rho f(\hat{u}_i - u_i) \qquad (2.2.1)$$

Where x_i (i = 1,2,3) or (x,y,z) are the Cartesian coordinates, u_i or (u,v,w) are the Cartesian components of the velocity vector. t, p, ρ, g, f represent time, pressure, density, gravity and the body force function respectively. $\hat{u}_i$ are the Cartesian components of the theoretical incident undisturbed wave orbital velocities. τ_{ij} is the stress tensor.

In case of differences in the undisturbed wave field (due to waves scattering from the ship) the body forces become active and the CFD solution is slowly forced towards the undisturbed wave solution as the waves propagate through the absorption zone. This technique is similar to the one presented by Peric and Abdel-Maksoud[2], with the following differences:

- Body forces are only applied to the momentum equations, not to the equation for the volume fraction which was found to be unnecessary.
- Peric and Abdel-Maksoud apply the body forces proportionally to the total velocity field instead of to the difference with the undisturbed wave. In this way the solution is forced to the calm water solution. This means however that the absorption zone cannot be used between ship and inflow boundary because it would affect the incident waves. This is an important limitation, especially for small ship speeds, where scattered waves may propagate towards the inflow and must be absorbed. For this reason, the implementation of the absorbing zones in ReFRESCO forces the flow towards the undisturbed wave.

The absorption zone definition consists of inner and outer ellipses. Inside the inner, small ellipse, no body-forces are applied. In the region between the inner and outer ellipses, the body-force magnitude is gradually increased and reaches its maximum

value at the outer ellipse. Beyond the outer ellipse, the body-force magnitude remains constant.

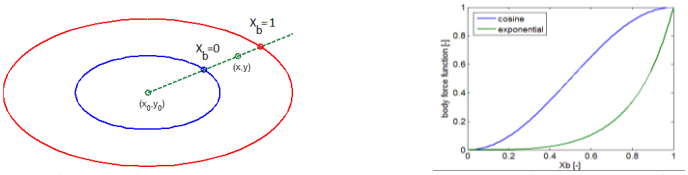

Figure 3 Definition of inner (blue) and outer (red) ellipse and body force variation functions.

The ellipses definition follows this formulation:

$$\left(\frac{x-x_0}{r_x}\right)^n+\left(\frac{y-y_0}{r_y}\right)^n=1 \quad (2.2.2)$$

where:

(x_0, y_0): ellipse centre

(r_x, r_y): ellipse radius

n: ellipse order (even number)

Increasing *n* transforms the ellipses into a near-rectangle. The ellipses are defined in a plane perpendicular to the gravity direction. The variation of the body force function between the edge of the inner and outer ellipse is defined by either a harmonic or an exponential function (see respectively Eq. 2.2.2 and 2.2.3).

$$f=\frac{\frac{1}{T_{ref}}\times f_{max}(1-\cos(\rho x_b))}{2} \quad (2.2.3) \qquad f=\frac{1}{T_{ref}}\times f_{max}\frac{e^{x_b^{3.5}}-1}{e^1-1} \quad (2.2.4)$$

Where X_b follows from a coordinate transformation and takes on value zero at the inner ellipse and one at the outer ellipse and varies along a line through the origin and the two intersecting points on the ellipses, see **Figure 3**. T_{ref} is a reference period, typically the wave period. f_{max} is the maximum body force value, which is dimensionless due to the use of the reference period in the body force formulation. This implies that the value of f_{max} is in principle independent of the wave period considered in the simulations, as long as the distance between the two ellipses is related to the length of the wave. The simulations performed in this paper make use of the exponential function, and the undisturbed regular waves prescribed in the domain follow the fifth-order Stokes wave formulation.

2.3. 2D wave post-processing

During the simulation, the free-surface elevation is monitored at 400 locations evenly spread inside the domain. From the monitored wave elevations, the variations in wave amplitudes and wave lengths along the domain as well as the amount of wave reflections are quantified. These quantities are analyzed within the inner-ellipse, i.e. outside the absorbing zone. A special attention is brought to these quantities to assess the three following aspects: (1) is the wave dispersion small enough such that the wave length is constant over the domain length and agrees with the wave length calculated from the dispersion relation? (2) is the wave dissipation small enough such that the wave height is constant over the domain length? (3) are the wave absorbing zones effective enough to limit the amount of wave reflections to a couple of percents?

To analyse the wave dispersion, the wave length is calculated at each time-step based on a spatial zero-up crossing analysis in a limited special window where the

wave elevation is not yet affected by possible wave reflection. The wave dispersion is then reported as the maximum relative error compared to the theoretical wave length obtained from linear theory. The wave height dissipation and the wave reflection are based on the recorded wave crest heights over the last two periods. The dissipation per wave length is then computed based on the mean slope of the crest height over the domain. It is reported as relative change of crest height over one wave length. The reflection coefficient is based on the maximum and minimum of the obtained wave crests heights see Eq. 2.3.1[3]. It is noted, that because reflection might be influenced by dissipation, the mean crest values are corrected for the dissipation.

$$C_r = \frac{H_{max} - H_{min}}{H_{max} + H_{min}} \tag{2.3.1}$$

3. Flow solver and discretisation settings

The simulations performed in this paper are done with the URANS solver ReFRESCO. ReFRESCO is a community based open-usage/open-source CFD code for the Maritime World. It solves multiphase unsteady incompressible viscous flows using the Navier-Stokes equations, complemented with turbulence models, cavitation models and volume-fraction transport equations for different phases. The equations are discretised using a finite-volume approach with cell-centred collocated variables, in strong-conservation form, and a pressure-correction equation based on the SIMPLE algorithm is used to ensure mass conservation.

A three-time level discretization scheme (2^{nd} order) with a fixed time-step is used for all equations. For convection schemes a QUICK scheme (2^{nd} order) is used for the momentum equations and the compressive scheme REFRICS is used for the free-surface. Within each time step a RMS residual drop below 10^{-4} nominal value is used for all equations unless indicated otherwise. Laminar calculations are conducted so the turbulence equation is not solved.

4. Sensitivity study

For the sensitivity study, a two-dimensional empty domain (i.e. no vessel inside) is used. The domain is 8λ long and 6λ high. The water depth amounts 3λ – which is larger than 0.5λ so deep water approximation is valid – and the still water level is therefore located at the middle of the domain. The simulations are performed for all waves described in **Figure 4**. The wave boundary condition is used both at the inlet and outlet of the domain following the fifth-order Stokes formulation. As shown in **Figure 2**, the width of the absorption zone is 1λ, and the outer-ellipse coincides with the outer boundaries of the domain. An absorption coefficient f_{max}=12 is used unless stated otherwise.

Wave frequency ω [rad/s]	Wave period T [s]	Wave length λ [m]	Wave amplitude ζ_a [m]	Wave steepness [-]
0.5	12.56	246.55	0.75	0.006
			1.5	0.012
			3.0	0.024
			6.0	0.049
			12.0	0.097

Figure 4 Properties of the simulated regular waves

4.1. Space and time discretisation at zero speed

The two-dimensional wave computations are conducted for five systematically refined unstructured grids generated with the grid generation package Hexpress and for five different time steps. The grid characteristics and the simulation matrix are listed in **Figure 5**. The following CFL numbers are given based on smallest cell size and the theoretical wave velocity. Because, the smallest cell size is at the free surface and is proportional to the wave amplitude, the given CFL numbers are independent of the wave amplitude. Also, it is noted that the cases with a CFL number above 0.3 are not reported since it was not possible to properly converge these simulations. Therefore for all wave heights the combination of grid 5 with T/100 and T/150 are neglected. With Grid-5 and for T/200, the 6.00 m and 12.0 m wave amplitude showed convergence issues.

Grid number		**1**	**2**	**3**	**4**	**5**
N_{Cells} / ζ_a in zone A (free surface)		2	3	5	6	9
N_{Cells} / λ in zone B (depth 0.2 λ)		24	32	48	64	96
N_{Cells} / λ in zone C (depth 0.6 λ)		12	16	24	32	48
Time step Δt	**T/100**	CFL = 0.13				CFL = 0.57
	T/150		CFL = 0.13			CFL = 0.38
	T/200			CFL = 0.16		CFL = 0.28
	T/300				CFL = 0.13	CFL = 0.19
	T/400	CFL = 0.03	CFL = 0.05	CFL = 0.08	CFL = 0.09	CFL = 0.14
Number of cells	ζ_a = 0.75 m	7572	10864	19560	29888	58896
	ζ_a = 12.0 m	4500	6768	13224	21440	44880

Figure 5 Grid characteristics for the 5 wave amplitudes and tested cases

Figure 6 summarizes the wave dispersions and dissipations analyzed from the monitored wave heights. The grids and time steps are represented on the horizontal axis while the dispersion and the dissipation are represented on the vertical axis. These results show that both the dispersion and dissipation results converge well when numerical settings are refined. Moreover, the dispersion error is more sensitive to the grid refinement than the time step refinement, although all grids and time steps show similar results for the two largest wave amplitudes. For the two largest waves, a relatively dispersion error is obtained for all gird and time steps. This is directly related to the fact that the present dispersion error is based on linear theory, and these steeper wave deviate from this simpler theory. Based on these results, it is concluded that the Grid-1 and Grid-2 are too coarse as they lead to large dissipation values. The combination of Grid-3 with a timestep T/200 is considered as the most efficient configuration, leading to dissipation between -0.2% and -0.8%.

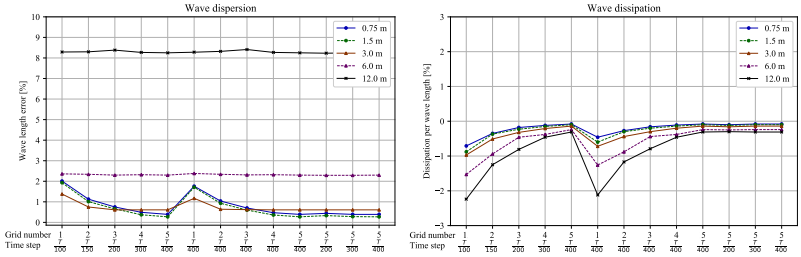

Figure 6 Wave dispersion and dissipation results without forward speed in deep water.

4.2. Effect of forward speed

To assess the effect of forward speed on the wave dispersion and dissipation, a similar study is performed with a forward speed of 10 knots. To account for the forward speed, the timestep is now based on the encounter period T_e. The CFLs obtained for the steepest wave are presented in **Figure 7**. The Grid-5 with timestep T/100 and T/150 lead to CFLs greater than 0.3, resulting in insufficient iterative convergence and are therefore neglected.

Figure 8 shows the wave dispersion and dissipation results. The trend of the results with forward speed is similar to the one at zero speed. The obtained dispersion is lower with forward speed than at zero-speed. However, more dissipation is obtained in this case. In particular, with Grid-3 and Δt = Te/200, which was chosen as best compromise for zero speed, dissipation between -1.1% and -1.4% is obtained. Going to the finest time step and finest grid, the dissipation values decreases towards 0.5%.

Grid number		1	2	3	4	5
Time step Δt	**Te/100**	CFL = 0.11				CFL = 0.45
	Te/150		CFL = 0.10			CFL = 0.30
	Te/200			CFL = 0.12		CFL = 0.22
	Te/300				CFL = 0.10	CFL = 0.15
	Te/400	CFL = 0.03	CFL = 0.04	CFL = 0.06	CFL = 0.07	CFL = 0.11

Figure 7 Grid characteristics for the 5 wave amplitudes and tested cases

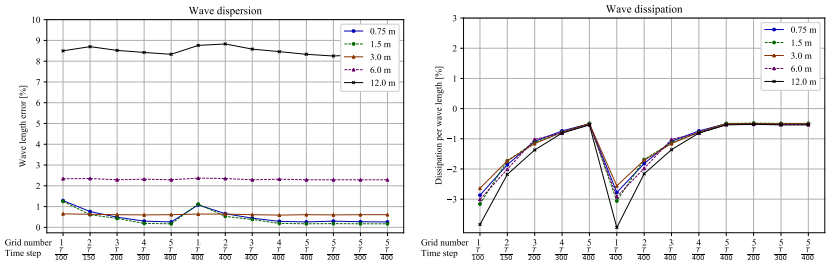

Figure 8 Wave dispersion and dissipation results with forward speed (10 knots).

4.3. Reflection coefficient in deep water

To assess the reflection from the downstream boundary, 66 simulations have been carried out for 3 wave frequencies (0.50 rad/s, 0.75 rad/s and 1.00 rad/s), 2 time steps (Te/200 and Te/800) and 3 forward speeds (0.0 kn, 5.0 kn, and 10.0 kn). A wide range of maximum absorption f_{max} is also covered. All simulations are carried out in a 2D domain similar to the one described in the previous section.

Figure 9 summarizes the reflection coefficients analyzed from all simulations. The results show that the minimum wave reflection is obtained for f_{max} values between 10 and 50 for all cases. In this range, all reflection coefficients are well below 1.0 %, except for the shortest wave which present a minimum wave reflection of 1.2%. This shows that assuming $T_{ref} = T_{wave}$ in the normalisation of damping body force leads to an f_{max} which is independent of the wave frequency and the time step. Similar results were already showed by Peric and Abdel-Maksoud [2].

At forward speed, the velocity of the reflected wave is not necessarily larger than the forward speed imposed. For this reason, the obtained wave reflections are more limited. Still, considering f_{max} values between 10 and 50 also leads to good results.

Finally, the present results confirm that the previous sensitivity studies were relatively free of reflection issues as they were all performed with f_{max} = 12.0.

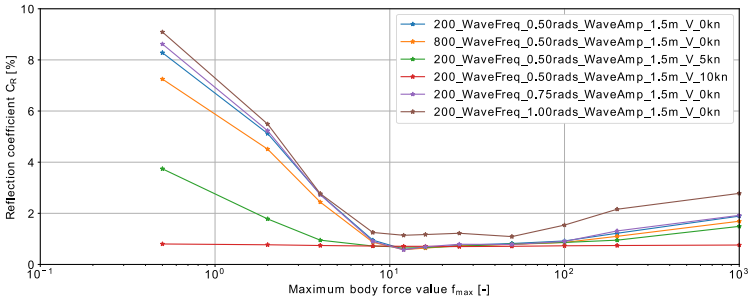

Figure 9 Wave reflection coefficient C_R as function of the maximum body force value

4.4. Extension to shallow water

The sensitivity analysis carried out in the previous sections were performed for deep water configurations. In this section, the focus lies on shallow water effects on the wave dispersion and dissipation. The objective is to determine if the settings used in shallow water yield to the same dispersion and dissipation as in deep water.

The computations with shallow water waves are carried out for two wave amplitudes of 0.75 m and 1.50 m. A water depth of 15.0 m is selected, leading to a wave length of 142m. The water depth is about 10% of the wave length, i.e. much lower than 50% of the wave length commonly used as a criterion to defined shallow water waves. Although the grid topology and refinement strategy are the same as in deep water, the CFL numbers are different because of the effects of the water-depth on the wave kinematics. The obtained maximum CFLs for the different time steps are presented in **Figure 10**.

Grid number		**1**	**2**	**3**	**4**	**5**
Time step Δt	**T/100**	CFL = 0.13				CFL = 0.50
	T/150		CFL = 0.13			CFL = 0.34
	T/200			CFL = 0.13		CFL = 0.25
	T/300				CFL = 0.10	CFL = 0.17
	T/400	CFL = 0.03	CFL = 0.05	CFL = 0.06	CFL = 0.08	CFL = 0.13

Figure 10 Grid characteristics for wave amplitudes 0.75 and 1.5 m and tested cases

Figure 11 shows the dispersion and dissipation results. The resulting dissipation for both wave amplitudes is within 1% and follow a similar trend as the deep-water case. The dispersion shows the same behaviour. However, it can be noted that the amount of reflections obtained in shallow water is somewhat larger than in deep water, increasing from less than 1% to about 3%.

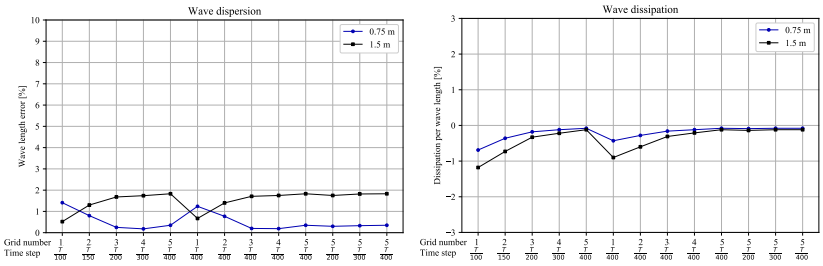

Figure 11 Wave dispersion and dissipation results.

5. Application to a 2D section in beam-on wave

One of the most important applications of the wave generation capabilities in CFD is to be able to calculate the motions of ships and platforms in waves. The main advantage of CFD compared to potential flow methods commonly used in the industry is to be able to account for non-linearities and viscous effects. As an application of the guidelines presented in this paper, the motions of a two-dimensional rectangular shaped hull section in beam-on waves are calculated. The hull section is equipped with two rectangular shaped bilge keels, is connected to a soft-spring mooring to keep the hull in place during the calculation. The motions are calculated for the sway, heave and roll degrees of freedom and are compared to results of potential flow theory.

The hull geometry and water depth considered in this study are such as used in the non-linear roll Joint Industry Project and are indicated in **Figure 12**. One regular wave of amplitude 0.01335 m and period 1.73 s is considered. The water depth is 0.9 m, which is 22 % of the modelled wave length, which means that shallow water can be expected. The domain and grids were made following the guidelines previously presented in this paper. Similarly to the simulations performed in the sensitivity study, no turbulence model is included for these computations. The main focus is to investigate the effect of numerical settings on the wave reflections and statistical convergence of the calculated motions and turbulence is not expected to have a major influence on this. Deforming grid algorithms are used to allow the hull to move in the domain while side boundaries are fixed. Forty wave periods are calculated, which gives sufficient data to analyse the motion response in a reliable manner. The regular wave is generated at the inlet using the 2nd order Stokes wave formulation. At the start of the computations, the incoming wave field is initialized in the whole domain. The boundary conditions or f_{max} coefficient in the absorbing zone are varied in order to investigate the effect of wave absorbing methods on the calculated motions. From the monitored motion time traces, the motion RAOs are derived by harmonic analysis.

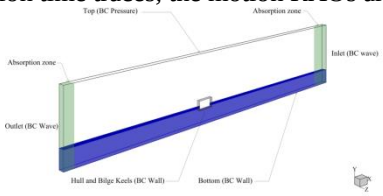

Property	Magnitude
Length	0.7269 m
Draft	0.187 m
Thickness	0.100 m
Depth	0.448 m
Water Depth	0.900 m
Width Absorbing Zone	1λ

Figure 12 Computational domain and boundary conditions used for the computations.

Although not presented in this paper, the grid and time step refinement studies have been conducted to make sure that the calculated motions were not affected significantly by discretisation errors. The calculated motion time traces for the optimal grid and time step are plotted in **Figure 13** for the different wave absorption coefficients investigated. The effect of the soft-mooring on the sway motions is clearly visible as it consists of both a low frequency motion occurring at the sway natural period of the hull, and a wave frequency signal which is due to the incoming wave. After the transient effects have disappeared and that the hull reached the mean sway offset, the calculated motions show a steady harmonic behaviour. This Figure shows that the motions are independent on the wave absorption methods in the first part of the calculation, i.e. before wave reflections at the side boundaries occur. Clear differences can be observed after ten wave periods though, which suggests that wave reflections affect the calculated motions if the waves are not correctly absorbed. This can also be

observed on the motion RAO shown in **Figure 13** and that are calculated from the time traces using harmonic analysis.

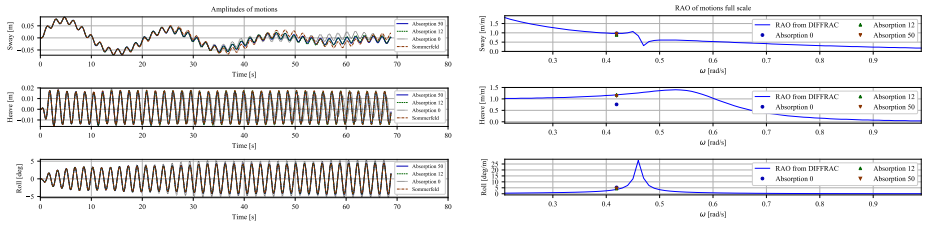

Figure 13 Effect of the absorbing methodology on the calculated motions in waves.

6. Conclusion

In this paper a specific attention is brought to the quality of the wave propagation in a two-dimensional domain. Based on considerations from linear wave theory, a grid topology involving the refinement of three different zones has been proposed. The objective of the proposed topology is to solve accurately the propagation of the wave kinetic energy not only near the free surface, but also up to 0.6λ below the undisturbed water-surface where 99.9% of the kinetic energy is transported.

The proposed grid topology was demonstrated for different waves propagating in an empty domain with or without forward speed, and in both deep and shallow water. Grid and timestep sensitivity studies were conducted to quantify the effect of discretization errors on the dissipation, dispersion and wave reflections. The results show that at deep water and zero-speed the dissipation, dispersion and reflections could all be brought within 1% when optimal settings were used. The wave dispersion increases and the wave dissipation decreases slightly when forward speed is modelled. Simulations in shallow water lead to an increase in the reflections up to 3%.

Based on these findings, the guidelines were applied to calculate the motions of a hull section in beam-on waves. Good results are obtained when waves are correctly absorbed at the domain boundaries. The motions are significantly affected by wave reflections though when no absorbing boundary is used.

7. Acknowledgements

The authors would like to thank the TKI Consortium for their financial support.

8. References

[1] www.refresco.org

[2] Peric, R. and Abdel-Maksoud, M., 2016. “Reliable Damping of Free Surface Waves in Numerical Simulations”. *Ship Technology Research.* 63. 10.1080/09377255.2015.1119921

[3] Ursell, F., Dean, R. G. and Yu, Y. S. 1960. Forced small-amplitude water waves: a comparison of theory and experiment, *Journal of Fluid Mechanics*, 7, (01), 33-52.

[4] Vaz, G., Jaouen, F. and Hoekstra, M., “Free Surface Viscous Flow Computations. Validation or URANS code FresCo”. *OMAE2009-79398.*

[5] Bandringa, H. et al., “Validation of CFD for run-up and wave impact on a semi submersible”. *Proceedings of 3rd International Conference on Violent Flows, 2016.*